**Philippine Journal of Science**
153 (5): 1945-1958, October 2024
ISSN 0031 - 7683
Date Received: 12 Apr 2024

# Extensions to the Su-Schrieffer-Heeger Model: Linear Chains and Their Topological Properties

**Dyn Paulo C. Dasallas* and Eduardo C. Cuansing**

Institute of Physics, University of the Philippines Los Baños,
College, Laguna 4031, Philippines

**The Su-Schrieffer-Heeger (SSH) model describes the dynamics of spinless fermions in a one-dimensional lattice, with sublattices $A$ and $B$, and governed by staggered hopping potentials $v$ and $w$ representing the intracell and intercell hopping energies, respectively. In this study, we extend the SSH model into three distinct types – a trimer chain, the generalized trimer chain, and a hexagonal chain. The trimer chain involves three sublattices with intracell and intercell hopping potentials $v$ and $w$, respectively. The generalized trimer chain incorporates the intracell hopping $v_1$ and $v_2$ and intercell hopping $w_1$ and $w_2$ to differentiate the hopping energies between different sublattices in the chain. The hexagonal chain is composed of six sublattices with intracell hopping potential $v$ and intercell hopping potential $w$. We utilize exact diagonalization to determine the bulk eigenvalues of the different models. We find that in the trimer and generalized trimer chain, the bulk eigenvalues exhibit conducting characteristics, independent of the hopping parameter, owing to the presence of a flat band situated along the Fermi energy. In the hexagonal chain, the bulk eigenvalues display semi-metallic characteristics in the region $v < w$ and metallic when $v = 0$. Furthermore, we investigate the presence of conducting edge states in the finite chains. The trimer and hexagonal chains show the presence of topologically protected edge states which are manifestations of one-dimensional topological insulators. We also established the bulk-boundary correspondence to calculate the winding number that predicts the existence of localized edge states in the topological nontrivial phase.**

Keywords: edge states, Su-Schrieffer-Heeger model, topological insulators, topological phase transition

## INTRODUCTION

Recently, topological insulators (TIs) gained a lot of attention due to their unique electrical properties as opposed to regular insulators. TIs are materials that have an energy band gap between the valence band and conducting band but have gapless edge states in one and two dimensions and surface states for 3D TIs (Asboth *et al*. 2015). The different phases of matter can be classified according to Landau's theory of symmetry breaking (Hasan and Kane 2010), which states that the different phases are due to their differences in symmetry. Furthermore, a phase transition occurs when there is a transition that changes the symmetry of the system (Wen 2004). However, the classification of phase transitions in TIs is beyond Landau's theory. This means that TIs can have different phases at zero temperature without breaking symmetry and the absence of classical phase transitions (Wen 2004). To differentiate these phases, we describe them by means of topological order (Guo 2016). These topological orders are generalized properties of zero temperature states having a finite band gap and do not change unless the system passes through a quantum phase transition, which is a singularity in the ground-state energy as a function of the parameters in the Hamiltonian (Wen 2004), as the temperature is increased. Furthermore, TI's also gained attention due to their possible applications in spintronics and quantum computing (Moore 2010).

*Corresponding author: dcdasallas@up.edu.ph

While most TI's are studied in two and three dimensions, one-dimensional models give us a good arena to study because of their reduced complexity and accessibility to experiments (Guo 2016). A good toy model for understanding TIs is the Su-Schrieffer-Heeger (SSH) model (Su *et al.* 1979). The SSH model describes the hopping of spinless fermions in a 1D lattice with staggered hopping potentials. It has a topological invariant winding number that shows the existence of edge states and differentiates the insulating phases through a quantum phase transition (Asboth *et al.* 2015). The SSH model was first applied in the study of the trans configuration of polyacetylene, which is the simplest conjugated polymer with alternating single and double covalent bonds (Su *et al.* 1979). Each of the carbon atoms in the chain forms four covalent bonds. One is with the hydrogen atom and three are with the neighboring carbon atoms. The SSH model can be used to find out the properties of spinless fermions in a chain such as *trans*-polyacetylene with alternating double and single bonds, represented by $v$ and $w$, as shown in Figure 1.

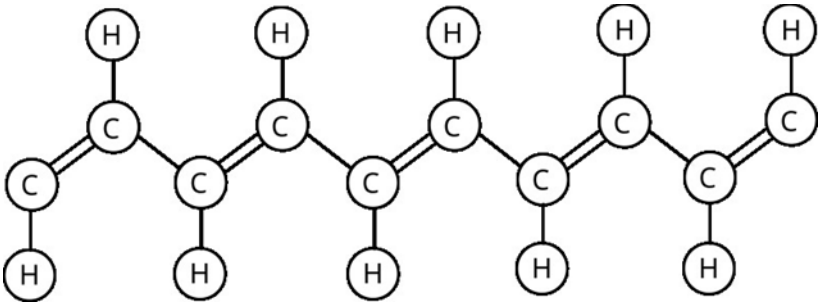


**Figure 1.** The trans configuration of polyacetylene.

Recent theoretical extensions of the SSH model include a 1D tripartite chain (Bercioux *et al.* 2017), 2D systems in square lattices (Obana *et al.* 2019), and arm-chair and zigzag graphene nanoribbons (Fujita *et al.* 1997). In this study, we extend the 1D SSH model into a tripartite chain and a hexagonal chain. We then determine the eigenstates and eigenvalues, *i.e.* the band structure of the extended models, and establish the bulk-boundary correspondence to find out if topological edge states are present in the models. We introduce our models in Sec. II and investigate their corresponding eigenstates, energy spectra, and winding numbers in Section III.

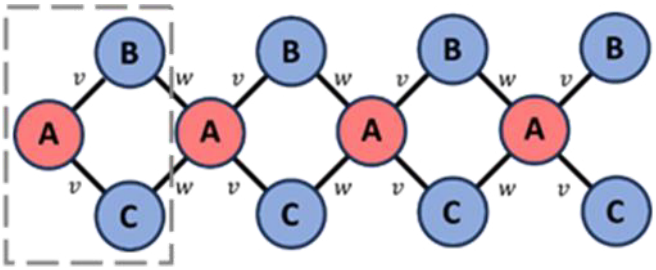


**Figure 2.** The trimer chain. A single unit cell is composed of three sublattices $A, B$, and $C$ and is connected by the hopping energies $v$ and $w$. A unit cell is shown enclosed in a box.

## THEORETICAL MODELS

### Trimer Chain

The trimer chain (see Figure 2) is composed of three sublattices $A$, $B$, and $C$ arranged in a diamond chain with staggered hopping potentials $v$ and $w$ accounting for the intracell and intercell hopping energies, respectively. The single particle Hamiltonian for this trimer chain is given by:

$$H = \sum_{m=1}^{N} v(\ |m,B\rangle\langle m,A|\ +\ |m,C\rangle\langle m,A|\ + h.c.\ ) + \sum_{m=1}^{N-1} w(|m+1,A\rangle\ \langle m,B|$$
$$+\ |m+1,A\rangle\langle m,C|\ + h.c.\ ) \tag{1}$$

where $m$ is the cell index, $v$ and $w$ are the hopping potentials, and h.c. denotes hermitian conjugation. This gives the matrix elements $H_{ij\,\alpha\,\beta} = \langle i,\ \alpha\ |\hat{H}|j,\ \beta\ \rangle$, where the indices $i,j = 1,2,3,\ldots N$ denote the cell number and $\alpha$, $\beta = A,B,C$ denote the sublattice index. We also set the on-site potential to zero, *i.e.* $H_{i=j,\,\alpha=\beta} = 0$. Furthermore, electron-electron interactions are neglected.

For the bulk, we set the boundary condition to be periodic, *i.e.* the Born-Von Karman condition. We consider an effectively infinitely long chain because of the periodic boundary condition. This also implies that the bulk now is translationally invariant, and Bloch's theorem holds (Asboth *et al.* 2015). Our bulk Hamiltonian with the periodic boundary condition reads:

$$H_{bulk} = \sum_{m=1}^{N} v(|m,B\rangle\langle m,A|\ +\ |m,C\rangle\langle m,A|\ + h.c.\ )$$
$$+ \sum_{m=1}^{N} w(\ |\ (m \bmod N)+1,A\rangle\ \langle m,B|\ +\ |(m \bmod N)+1,A\rangle\langle m,C|\ + h.c.\ ) \tag{2}$$

To account for the periodicity, we introduce terms for the hopping between sites $1A$ and $NB$, $1A$ and $NC$, and *vice versa*.

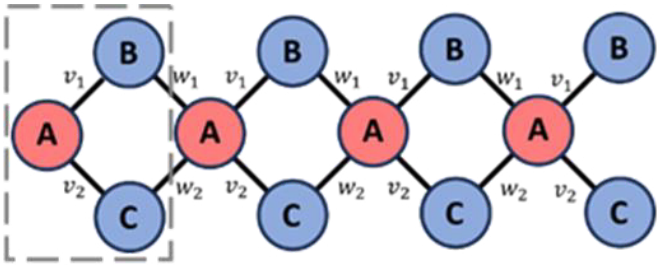


**Figure 3.** The generalized trimer chain. A single unit cell is composed of three sublattices A,B, and C and connected by the hopping energies $v_1$,$v_2$,$w_1$ and $w_2$. A single unit cell is shown enclosed in a box.

**Generalized Trimer Chain**

The generalized trimer chain is a generalization of the trimer chain introduced in Sec. II A. This model differentiates intracell and intercell hopping energies for $AC$, *i.e.* site $A$ to site $C$ in the same unit cell, and $AB$, *i.e.* site $A$ to site $B$ in the same unit cell and $BA$, *i.e.* site $B$ to site $A$ in the neighboring unit cell, and $CA$, *i.e.* site $C$ to site $A$ in the neighboring unit cell, hopping energies (see Figure 3). The single-particle Hamiltonian for this model is:

$$H = \sum_{m=1}^{N} v_1(|m,B\rangle\langle m,A|+h.c.\ ) + \sum_{m=1}^{N-1} v_2(|m,C\rangle\langle m,A|+h.c.\ )$$
$$+ \sum_{m=1}^{N-1} w_1(|m+1,A\rangle\ \langle m,B|\ +\ h.c.\ ) + \sum_{m=1}^{N-1} w_2(\ |m+1,A\rangle\langle m,C|\ + h.c.\ ). \tag{3}$$

For the bulk part of the chain, we model it as a chain with periodic boundary conditions. The Hamiltonian for the bulk is:

$$H_{bulk} = \sum_{m=1}^{N} v_1(|m,B\rangle\langle m,A| + h.c.) + \sum_{m=1}^{N} v_2(|m,C\rangle\langle m,A| + h.c.)$$

$$+ \sum_{m=1}^{N} w_1(|(m \bmod N)+1,A\rangle\langle m,B| + h.c.) \quad (4)$$

$$+ \sum_{m=1}^{N} w_2(|(m \bmod N)+1,A\rangle\langle m,C| + h.c.). \quad (4)$$

The The additional terms in the Hamiltonian account for the periodicity of the bulk.

Similar to the work of Bercioux *et al.* (2017), we calculated the band structures of a tripartite lattice with infinite and finite unit cells. The Lattice I of their work is similar to our trimer chain with intercell hopping in the $A$, $B$, and $C$ sublattices. Our generalized trimer chain generalizes the tripartite system, which includes their Lattice II as a special case when $v_1 = w_2$ and $v_2 = w_1$. To highlight the novelty of our work, we will show the eigenstates of the finite chains in the topological nontrivial and trivial regime. We will also calculate the winding number to establish the bulk-boundary correspondence of our three model chains.

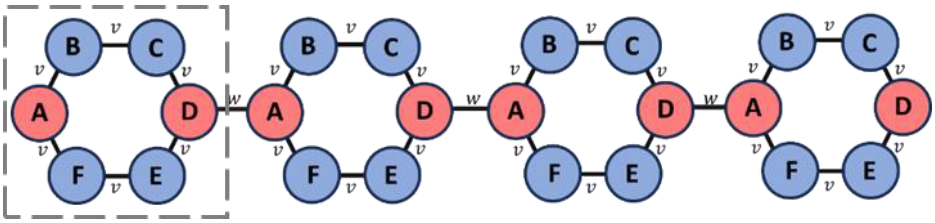


**Figure 4.** The hexagonal chain. A single unit cell is composed of six sublattices $A, B, C, D, E$, and $F$, and is connected by the hopping energy $v$ and intercell hopping energy $w$. A unit cell is shown enclosed by the box.

**Hexagonal Chain**

The hexagonal chain forms a resemblance to a 1D graphene armchair ribbon, as shown in Figure 4. It consists of six sublattices and staggered hopping potentials $v$ and $w$ for the intracell and intercell hopping, respectively. The single-particle Hamiltonian for this hexagonal chain is:

$$H = \sum_{m=1}^{N} v(|m,B\rangle\langle m,A| + |m,C\rangle\langle m,B| + |m,D\rangle\langle m,C| + |m,D\rangle\langle m,E| + |m,E\rangle\langle m,F|$$

$$+|m,F\rangle\langle m,A| + h.c.) + \sum_{m=1}^{N-1} w(|m+1,A\rangle\langle m,D| + h.c.) \quad (5)$$

(5)

where

where $m$ is the unit cell index. The elements of the Hamiltonian matrix are given by $H_{ij\alpha\beta} = \langle i, \alpha | \hat{H} | j, \beta \rangle$ where $i, j = 1,2,3 \ldots N$ and $\alpha, \beta = A, B, C, D, E, F$. The Hamiltonian for the bulk part of the chain modeled using periodic boundary conditions is:

$$H_{bulk} = \sum_{m=1}^{N} v(\ |m,B\rangle\langle m,A|\ +\ |m,C\rangle\langle m,B|+\ |m,D\rangle\langle m,C|+\ |m,D\rangle\langle m,E|+\ |m,E\rangle\langle m,F| \\ +\ |m,F\rangle\langle m,A|\ + h.c.)\ + \sum_{m=1}^{N} w\,|(m \bmod N)+1,A\rangle\,\langle m,D|\ + h.c.) \tag{6}$$

## EIGENVALUES, EIGENSTATES AND THE WINDING NUMBER

**Trimer Chain**

Considering the bulk Hamiltonian of the trimer chain in Equation 2, the energy eigenvalues of the system can be determined using exact diagonalization. The Schrödinger equation for the bulk Hamiltonian in matrix form is given by:

$$\begin{pmatrix} 0 & v+we^{-ik} & v+we^{-ik} \\ v+we^{ik} & 0 & 0 \\ v+we^{ik} & 0 & 0 \end{pmatrix}\begin{pmatrix} A(k) \\ B(k) \\ C(k) \end{pmatrix} = \mathrm{E(k)}\begin{pmatrix} A(k) \\ B(k) \\ C(k) \end{pmatrix}. \tag{7}$$

This gives the energy eigenvalues:

$$E_0(k) = 0 \text{ and } E_{\pm}(k) = \pm\sqrt{2(v^2+w^2+2vw\,cos(k))}, \tag{8}$$

where $k$ is the wave number taking up values in the first Brillouin zone (Asboth *et al.* 2015). There are three eigenvalues in Equation 8. The first eigenvalue (zero energy) has energy coinciding with the Fermi energy, *i.e.* $E_0(k) = 0 = E_f$ (Asboth *et al.* 2015). By varying the magnitude of the hopping parameters $v$ and $w$, a dispersion relation shown in Figure 5 can be obtained.

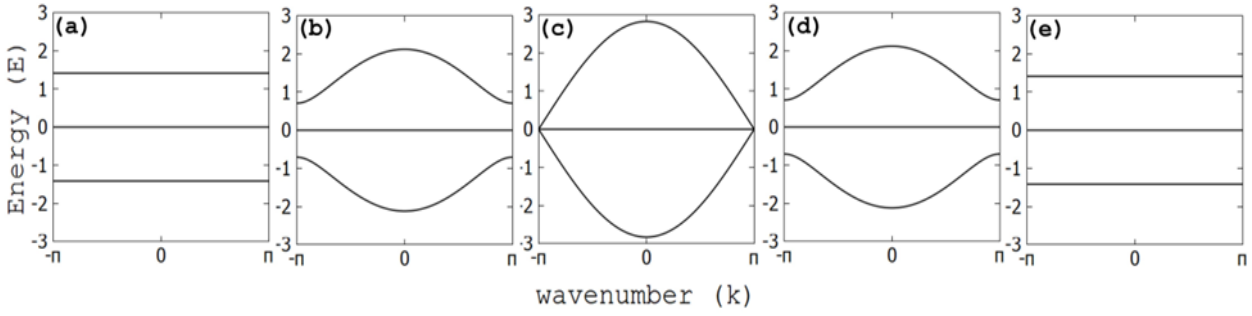


**Figure 5.** Bulk eigenvalues of the trimer chain plotted in the first Brillouin zone ($k = [-\pi, \pi]$) with Fermi energy $E_f = 0$: [a] $v = 1, w = 0$; [b] $v = 1, w = 0.5$; [c] $v = 1, w = 1$; [d] $v = 0.5, w = 1$; [e] $v = 0, w = 1$.

The dispersion relation consists of five different scenarios concerned with the different magnitudes of the hopping parameter. Figure 5a describes the system with $v = 1$ and $w = 0$. Examining the figure, it can be seen that there exists a flat band situated at the Fermi level $E = 0$. This is due to $E_0(k)$ which has a constant value and is independent of the wave number $k$. This characteristic can be seen in all the configurations indicating that all of the configuration of the system is a conductor (Simon 2013). Furthermore, two flat bands can also be observed at regions $E = \pm\sqrt{2}v$. The same observations can be seen in Figure 5e with flat bands situated at $E = \pm\sqrt{2}w$ for $v = 0$ and $w = 1$. The case for

$v > w$, Figure 5b and $v < w$, Figure 5d, show sinusoidal variations of the energy with respect to the wave number. A defined gap between the uppermost and the lowest energy band can be seen. Lastly, for the case where $v = w$, Figure 5c, the uppermost and the lowest energy band crossed in the region $k = \pm\pi$ indicating an intersection, at a point, between the two bands.

To consider the characteristics of the boundaries of the chain, we examine a finite trimer chain. For the extreme cases where $v = 0$ or $w = 0$, the chain breaks down into trimers. For the trivial case $w = 0$, it can be observed that all of the sites belong to a corresponding trimer. However, for the topological case where $v = 0$, there are sites that do not belong to a corresponding trimer. Since fermions in these sites do not hop, then these edge sites host zero-energy states given by $\hat{H}|1, A\rangle = \hat{H}|N, B\rangle = \hat{H}|N, C\rangle = 0$.

To calculate the eigenvalues of the finite trimer chain, we diagonalize the Hamiltonian given by:

$$H = \begin{pmatrix} A & B & 0 & \cdots & & & \\ B^T & A & B & 0 & \cdots & & \\ 0 & B^T & A & B & 0 & \cdots & \\ \cdots & & & & & & \cdots \\ & \cdots & 0 & B^T & A & B & 0 \\ & & \cdots & 0 & B^T & A & B \\ & & & \cdots & 0 & B^T & A \end{pmatrix} \tag{9}$$

with:

$$A = \begin{pmatrix} 0 & v & v \\ v & 0 & 0 \\ v & 0 & 0 \end{pmatrix} \text{ and } B = \begin{pmatrix} 0 & 0 & 0 \\ w & 0 & 0 \\ w & 0 & 0 \end{pmatrix}, \tag{10}$$

where for $N = 10$ unit cells, the Hamiltonian is a $30 \times 30$ matrix. By varying the hopping amplitude $v$ of the finite trimer chain, the eigenvalue spectra can be obtained (see Figure 6). As observed from Figure 6a, zero-energy states span throughout the graph independent of the values of $v$. This corresponds to the zero-energy eigenvalue that we calculated earlier for the bulk (see Equation 8). Notice that these states with zero energy are degenerate. In Figure 6a, there are 10 states having the same zero energy. Furthermore, in the region where $v < w$, there exist two additional zero-energy states that reside at the edges of the chain. These results are consistent with those found by Bercioux *et al.* (2017). This region is defined as the topologically nontrivial phase as opposed to the region where $v > w$, which we define as the topologically trivial phase. As we will see later in this section, these regions have different topological invariants that distinguish their topological phase. Additionally, a topological phase transition can be observed in the region where the hopping potentials are equal. Figures 6b and c show the probability density $|\Psi|^2$ for the corresponding unit cells. Figure 6b shows an arbitrary state where $E \neq 0$ wherein the probability density extends throughout the whole chain. In contrast, Figure 6c shows a state where $E = 0$. As seen in this plot, the probability density is localized on both the left and right edges of the chain. These states are defined as edge states, where the wave function is localized on both edges of the chain and exponentially decays into the bulk. These edge states are typical characteristics of a one-dimensional TI (Asboth *et al.* 2015).

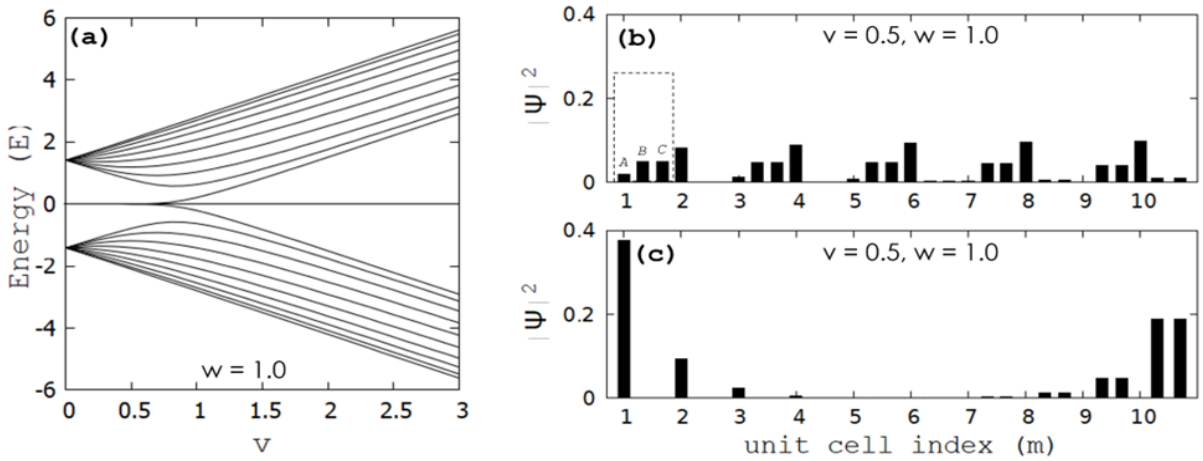


**Figure 6.** Eigenvalues and eigenstates of a finite trimer chain with N = 10: [a] energy of N = 10 unit cell trimer chain with varying v while keeping w=1; [b] probability density of an arbitrary nonzero energy state. A single unit cell is enclosed by the dashed line with sublattice A,B,C; [c] probability density of a zero-energy edge state.

**Generalized Trimer Chain**

Following the same procedure as in the previous section, we solve for the energy eigenvalues of the generalized trimer chain using exact diagonalization. The Schrödinger equation, using the bulk Hamiltonian in matrix representation is given by:

$$\begin{pmatrix} 0 & v_1 + w_1 e^{-ik} & v_2 + w_2 e^{-ik} \\ v_1 + w_1 e^{ik} & 0 & 0 \\ v_2 + w_2 e^{ik} & 0 & 0 \end{pmatrix} \begin{pmatrix} A(k) \\ B(k) \\ C(k) \end{pmatrix} = \mathrm{E(k)} \begin{pmatrix} A(k) \\ B(k) \\ C(k) \end{pmatrix}. \tag{11}$$

This gives the energy eigenvalues:

$$\begin{aligned} E_0(k) &= 0, \\ E_{\pm}(k) &= \pm\sqrt{v_1^2 + w_1^2 + 2v_1 w_1 \cos(k) + v_2^2 + w_2^2 + 2v_2 w_2 \cos(k)}. \end{aligned} \tag{12}$$

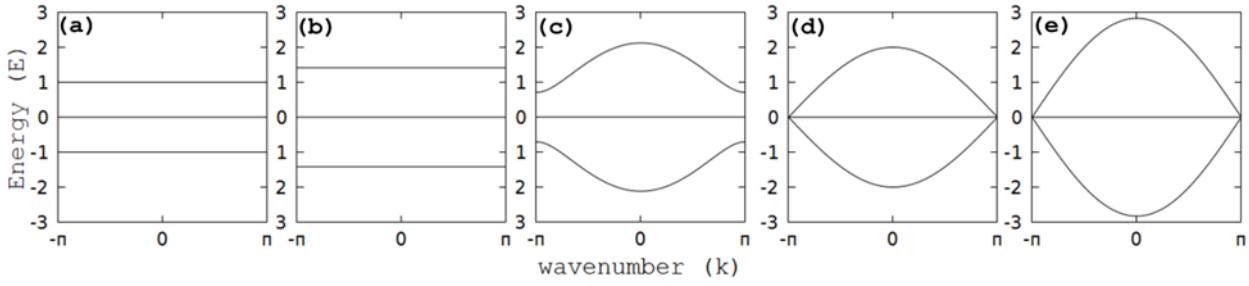


**Figure 7.** Bulk eigenvalues of the generalized trimer chain plotted in the first Brillouin zone (k=[-π,π]) with Fermi energy $E_f$=0: [a] $v_1$=1,$v_2$=$w_1$=$w_2$=0; [b] $v_1$=$v_2$=0, $w_1$=$w_2$=1; [c] $v_1$=0 ,$v_2$=$w_1$=$w_2$=1; [d] $v_1$=$w_1$=0, $v_2$=$w_2$=1; [e] $v_1$=$v_2$=$w_1$=$w_2$=1.

Notice that when we set $v_1 = v_2$ and $w_1 = w_2$, we will arrive at the same energy eigenvalues as those for the trimer chain in Equation 8. Shown in Figure 7 are the plots of the energy eigenvalues of the generalized trimer chain with respect to the wave number $k$. As seen from the plots, different combinations of the hopping potentials lead to the same conducting characteristics due to the flat band situated along the Fermi level. This band is due to $E_0(k)$ that we obtained. Furthermore, as expected, the configurations where $v_1 = v_2$ and $w_1 = w_2$ resembles the dispersion relations of the trimer chain shown in Figure 5c. A visible gap between the uppermost and lowest energy band can be seen in Figure 7c in the case where one hopping parameter is zero ($v_1 = 0$), whereas the rest are equal. It can be generalized that this band gap will remain open until we reach the limit where $v_1 = w_1$ and/or $v_2 = w_2$ (see Figures 7d and e).

To determine the characteristics of the finite generalized trimer chain, we consider a lattice composed of 10 unit cells. We find that when only one of the hopping potentials is nonzero and the rest are set to zero, the chain breaks down into dimers and the isolated sites would host zero-energy states. To calculate the eigenvalues of the generalized trimer chain, we diagonalize the Hamiltonian given by:

$$H = \begin{pmatrix} A & B & 0 & \cdots & & & \\ B^T & A & B & 0 & \cdots & & \\ 0 & B^T & A & B & 0 & \cdots & \\ \cdots & & & & & & \cdots \\ & \cdots & 0 & B^T & A & B & 0 \\ & & \cdots & 0 & B^T & A & B \\ & & & \cdots & 0 & B^T & A \end{pmatrix} \tag{13}$$

with

$$A = \begin{pmatrix} 0 & v_1 & v_2 \\ v_1 & 0 & 0 \\ v_2 & 0 & 0 \end{pmatrix} \text{ and } B = \begin{pmatrix} 0 & 0 & 0 \\ w_1 & 0 & 0 \\ w_2 & 0 & 0 \end{pmatrix}, \tag{14}$$

where for a $N = 10$ unit cell generalized trimer chain, the Hamiltonian is a $30 \times 30$ matrix. Figure 8a shows the eigenvalue spectra of the finite $N = 10$ generalized trimer chain by varying the three parameters $v_2 = w_1 = w_2$ simultaneously while maintaining $v_1 = 1$. Also, the topological nontrivial phase in the region $v < w$ which we found earlier in the trimer chain (see Figure 6a), motivated us to explore the generalized case where $(v_1 \neq v_2) < (w_1 = w_2)$. This case is shown in Figure 8b where we vary the value of $v_1$ in the range [0,3] while maintaining $v_2 = 0.5$ and $w_1 = w_2 = 1$. As noticed from Figure 8b, the states that form the edges in the trimer chain are now gapped in the region, where $v_1 < v_2$ and $v_1 > v_2$. This gap only closes in the trimer chain limit where $(v_1 = v_2) < (w_1 = w_2)$.

Figure 8c shows a representative probability density located at nonzero energy levels. Figure 8d shows the probability density of one of the degenerate states in the generalized trimer chain. Lastly, we examined the eigenstates in the region where $v_1 < v_2$, of which a representative probability density is shown in Figure 8e. Although these states are nonzero energy-gapped states, they display a unique characteristic, wherein the probability is only localized in one of the edges. They are known as chiral edge states (Martinez Alvarez and Coutinho-Filho 2019), which resemble only half of the full edge states of the original SSH model. As we will show later in this section, these chiral edge states do not share the same winding number as the gapless zero-energy edge states observed in the trimer chain.

To establish the bulk-boundary correspondence of the trimer and generalized trimer chain, we express their bulk momentum-space Hamiltonian in terms of the basis states. Consider the following traceless and hermitian matrices, which are four of the matrices known as Gell-Mann matrices representing the basis of the group SU(3) (Haber 2017):

$$\lambda_1 = \begin{pmatrix} 0 & 1 & 0 \\ 1 & 0 & 0 \\ 0 & 0 & 0 \end{pmatrix}, \lambda_4 = \begin{pmatrix} 0 & 0 & 1 \\ 0 & 0 & 0 \\ 1 & 0 & 0 \end{pmatrix}, \lambda_2 = \begin{pmatrix} 0 & -i & 0 \\ i & 0 & 0 \\ 0 & 0 & 0 \end{pmatrix}, \lambda_5 = \begin{pmatrix} 0 & 0 & -i \\ 0 & 0 & 0 \\ i & 0 & 0 \end{pmatrix}. \tag{15}$$

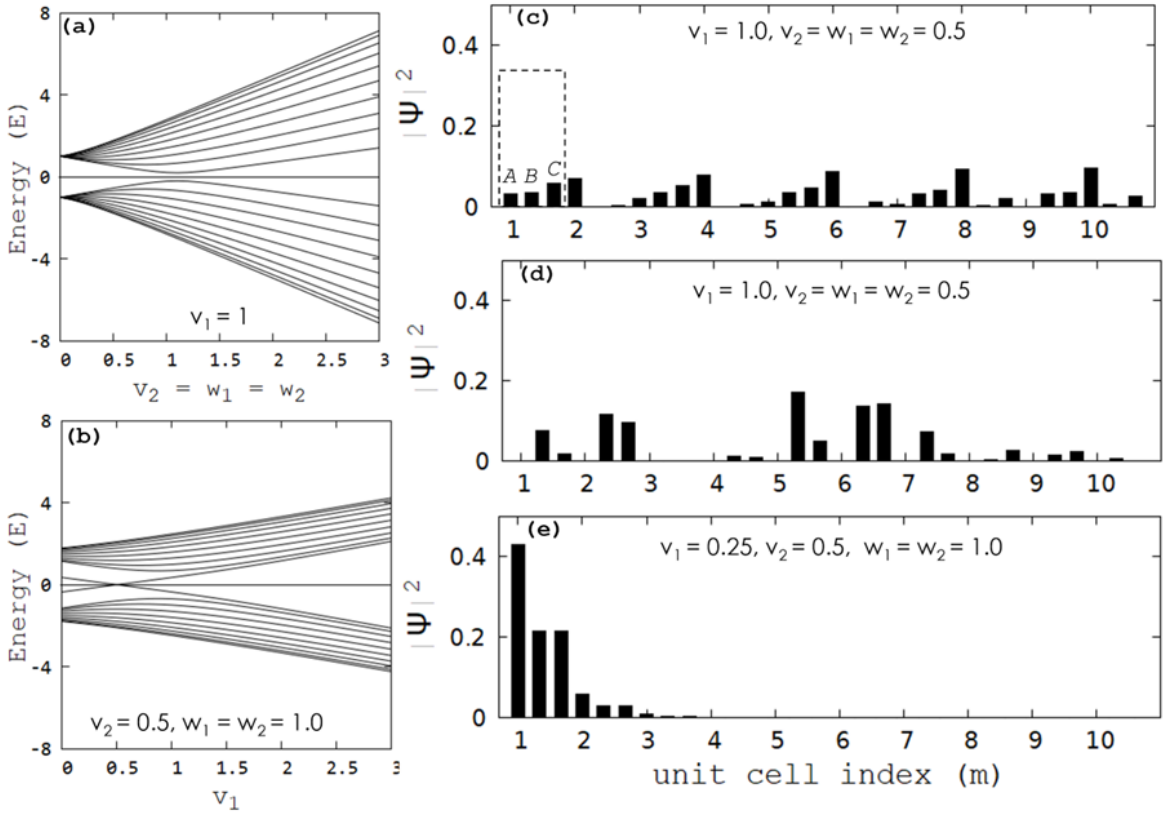


**Figure 8.** Eigenvalues and eigenstates of a finite generalized trimer chain with N = 10. [a] Energy of N = 10 unit cell generalized trimer chain with varying $v_2$=$w_1$=$w_2$ while keeping $v_1$=1. [b] Energy of N = 10 unit cell generalized trimer chain with $v_2$=0.5 and $w_1$=$w_2$=1 and with varying $v_1$. [c] Probability density of an arbitrary nonzero energy state. A single unit cell is enclosed by a dashed line with sublattice A,B,C. [d] Probability density of a zero-energy degenerate state. [e] Probability density of a chiral edge state.

The bulk-momentum space Hamiltonian of the trimer chain can then be expressed as:

$$H(k) = \sqrt{2}(v + w\cos(k))\ \Lambda_x + \sqrt{2}w\sin(k)\ \Lambda_y \tag{16}$$

in which the new basis $\Lambda_x$ and $\Lambda_y$ are linear combinations of the Gell-Mann matrices:

$$\Lambda_x = \frac{1}{\sqrt{2}}(\lambda_1 + \lambda_4),$$
$$\Lambda_y = \frac{1}{\sqrt{2}}(\lambda_2 + \lambda_5), \tag{17}$$

where the normalization coefficients ensure that the basis states follow the same trace orthonormality condition as that of the Gell-Mann matrices $\mathrm{Tr}[\Lambda_i \Lambda_j] = 2\,\delta_{ij}$ (Haber 2017). On the other hand, for the generalized trimer chain, the bulk momentum-space Hamiltonian can be expressed as:

$$H(k) = (v_1 + w_1\cos(k))\,\lambda_1 + (v_2 + w_2\cos(k))\,\lambda_4 + (w_1\sin(k))\,\lambda_2 + (w_2\sin(k))\,\lambda_5. \tag{18}$$

We can see that Eq. (18) reduces to Eq. (16) in the limit $v_1 = v_2$ and $w_1 = w_2$. To reduce the parameters imposed by the four-dimensional vector of the bulk momentum-space Hamiltonian of the generalized trimer chain, we set $w_1 =$

$w_2 = w$, *i.e.* effectively reducing the free parameters from four to three. The bulk momentum-space Hamiltonian of the generalized trimer chain now reads:

$$H(k) = (v_1 + w\cos(k))\,\lambda_1 + (v_2 + w\cos(k))\,\lambda_4 + (\sqrt{2}w\sin(k))\,\Lambda_y. \tag{19}$$

Note that the Hamiltonian in Equation 19 satisfies chiral symmetry with the corresponding chiral operator:

$$\Gamma = \begin{pmatrix} 1 & 0 & 0 \\ 0 & -1 & 0 \\ 0 & 0 & -1 \end{pmatrix} \tag{20}$$

where $\Gamma H(k)\,\Gamma^{\dagger} = -H(k)$ and $\Gamma^2 = 1$.

To calculate the topological invariant winding number, we project the bulk momentum-space Hamiltonians into their corresponding basis states. As for the Hamiltonian of the trimer chain in Equation 16, it has a resemblance with that of the bulk momentum-space of the original SSH dimer. As such, we expect its trajectory in the $\Lambda_x \Lambda_y$ space to look like the trajectory of the SSH Hamiltonian in the $dxdy$ space. From these trajectories, we can calculate the winding number $\nu$ by counting the number of times the trajectory orbits around the origin, *i.e.* around $\Lambda_x = \Lambda_y = 0$. We determine the following winding number $\nu$ for the trimer chain:

$$\nu = \begin{cases} 0, & v > w \\ \text{undetermined}, & v = w. \\ 1, & v < w \end{cases} \tag{21}$$

The winding number is a useful tool in predicting the existence of gapless localized edge states (states where the wave function of the system is localized on both edges of the chain) (Asboth *et. al* 2015). As shown in Equation 21, for the case where $v > w$, we found that $\nu = 0$, thus indicating a trivial topology of the system characterized by the absence of localized edge states. On the other hand, the case where $v < w$ indicates a nontrivial topology where $\nu = 1$, indicating the presence of a pair of gapless localized edge states. Furthermore, the case where $v = w$ leads to an undetermined $\nu$ indicating that the trajectory of $H$ is in direct contact with the origin. This case entails a topological phase transition, which shows that the only way to change the winding number of the trimer chain from $\nu = 0$ to $\nu = 1$, or vice versa, is by closing the gap between the highest and lowest band of the trimer chain.

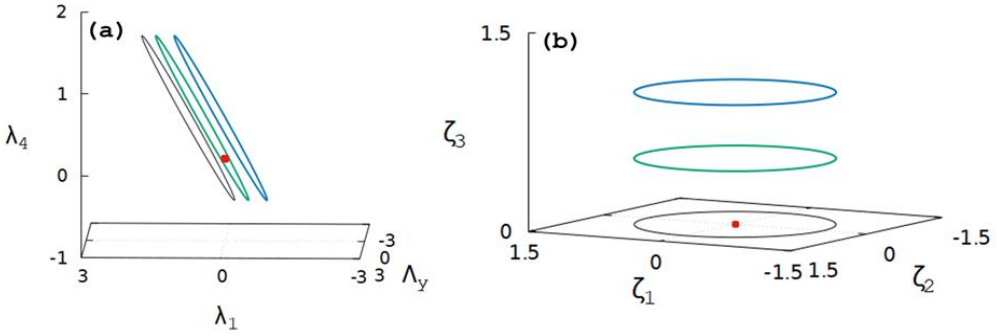


**Figure 9.** Trajectories of the bulk momentum-space Hamiltonian of the generalized trimer chain and hexagonal chain in the λ and ζ basis. [a] Trajectories of the bulk momentum-space Hamiltonian of the generalized trimer chain with varying ν. The red dot corresponds to the origin, i.e. $\lambda_1=\lambda_4=\Lambda_y=0$. The blue circle (rightmost) corresponds to the parameters $v_1=0.1, v_2=0.5, w_1=w_2=1$, where the winding number ν= 0, green circle (middle) with parameters $v_1=v_2=0.5, w_1=w_2=1$, where the winding number ν= 1 and the black circle (leftmost) with parameters $v_1=0.8, v_2=0.5, w_1=w_2=1$ where the winding number ν=0. [b] Trajectories of the bulk momentum-space Hamiltonian of the hexagonal chain with varying ν. The red dot corresponds to the origin, $\zeta_1=\zeta_2=\zeta_3=0$. The black circle (lowermost) corresponds to the parameters v= 0,w=1, where the winding number ν= 1, green circle (middle) with parameters v= 0.5 ,w=1, where the winding number ν= 0 and blue circle (uppermost) with v= w=1 where the winding number ν= 0.

Extending our analysis to the generalized case, we plot the trajectory of the bulk momentum-space Hamiltonian of the generalized trimer chain, Equation 19 in $\lambda$-space, as shown in Figure 9a. Here, we are interested to see if the winding number changes or remains the same for different variations in the upper, $v_1$, and lower, $v_2$, intracell hopping parameters. We are particularly interested in this case due to the nontrivial topological nature of the trimer chain in the $v < w$ regime, as we have shown earlier in this section. As such, we would like to generalize the conditions for the existence of gapless localized edge states in the $(v_1 \neq v_2) < w$ regime in terms of their winding numbers. As observed in Figure 9a, we determined the following winding numbers:

$$\nu = \begin{cases} 0, & v_1 > v_2 \\ 1, & v_1 = v_2 \\ 0, & v_1 < v_2 \end{cases} \tag{22}$$

where $w = 1$ for all cases. From this result, we can see that only in the trimer chain limit, *i.e.* $v_1 = v_2$, is the winding number $\nu = 1$ where we have shown a localized edge state in Figure 6c. It is also the region where the gap closes at $E = 0$ between the pair of positive and negative energy bands in Figure 8b. The other configurations on the other hand, in Equation 22, with $v_1 > v_2$, and $v_1 < v_2$, demonstrate a chiral edge state emerging from a nonzero energy state, which is quite different from the usual gapless localized edge states where the probability densities are localized on both of the edges of the chain (Martinez Alvarez and Coutinho-Filho 2019).

**Hexagonal Chain**

Solving for the bulk energy eigenvalues of the hexagonal chain requires us to solve Schrödinger's equation given by:

$$\begin{pmatrix} 0 & v & 0 & we^{-ik} & 0 & v \\ v & 0 & v & 0 & 0 & 0 \\ 0 & v & 0 & v & 0 & 0 \\ we^{ik} & 0 & v & 0 & v & 0 \\ 0 & 0 & 0 & v & 0 & v \\ v & 0 & 0 & 0 & v & 0 \end{pmatrix} \begin{pmatrix} a(k) \\ b(k) \\ c(k) \\ d(k) \\ e(k) \\ f(k) \end{pmatrix} = \mathrm{E(k)} \begin{pmatrix} a(k) \\ b(k) \\ c(k) \\ d(k) \\ e(k) \\ f(k) \end{pmatrix}. \tag{23}$$

The energy eigenvalues of the hexagonal chain with varying hopping parameters can be calculated by numerically diagonalizing the matrix in Equation 23. We do this using the GNU Octave computational tool software. The eigenvalues are shown in Figure 10.

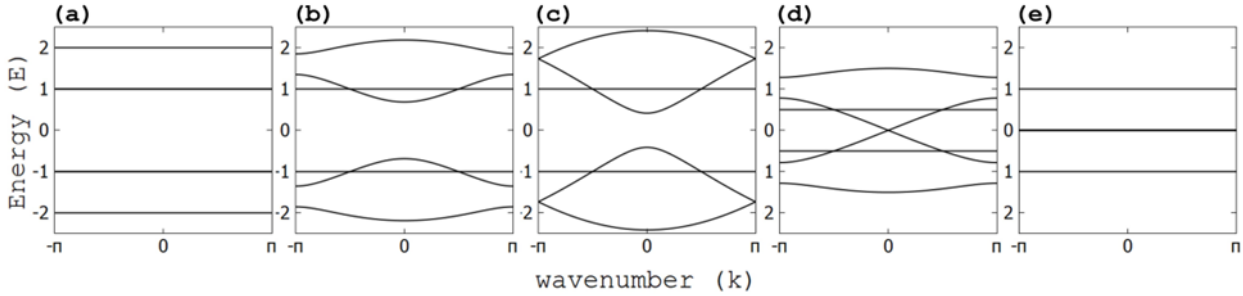


**Figure 10.** Bulk eigenvalues of the hexagonal chain plotted in the first Brillouin zone (k=[-π,π]) with the Fermi energy $E_f$=0: [a] v=1 ,w = 0; [b] v =1 ,w = 0.5; [c] v = w=1; [d] v=0.5,w=1; [e] v = 0, w=1.

We see that Figures 10a–c show an insulating system due to the presence of a band gap. Furthermore, in Figure 10d, where $v < w$, a conical band structure can be seen at $k = 0$. This band structure displays gapless and linear conducting

bands, which are typical for a semi-metal (Wan *et al.* 2011). Additionally, when $v = 0$, see Figure 10e, the chain shows conducting characteristics due to the flat band situated along the Fermi energy, $E_f = 0$, independent of the wave number $k$. The eigenvalue spectra can be determined by diagonalizing the Hamiltonian given by:

$$H = \begin{pmatrix} A & B & 0 & \cdots & & & \\ B^T & A & B & 0 & \cdots & & \\ 0 & B^T & A & B & 0 & \cdots & \\ \cdots & & & & & & \cdots \\ & \cdots & 0 & B^T & A & B & 0 \\ & & \cdots & 0 & B^T & A & B \\ & & & \cdots & 0 & B^T & A \end{pmatrix} \tag{24}$$

with:

$$A = \begin{pmatrix} 0 & v & 0 & 0 & 0 & v \\ v & 0 & v & 0 & 0 & 0 \\ 0 & v & 0 & v & 0 & 0 \\ 0 & 0 & v & 0 & v & 0 \\ 0 & 0 & 0 & v & 0 & v \\ v & 0 & 0 & 0 & v & 0 \end{pmatrix} \text{ and } B = \begin{pmatrix} 0 & 0 & 0 & 0 & 0 & 0 \\ 0 & 0 & 0 & 0 & 0 & 0 \\ 0 & 0 & 0 & 0 & 0 & 0 \\ w & 0 & 0 & 0 & 0 & 0 \\ 0 & 0 & 0 & 0 & 0 & 0 \\ 0 & 0 & 0 & 0 & 0 & 0 \end{pmatrix}, \tag{25}$$

where for a $N = 10$ unit cell hexagonal chain, the Hamiltonian is a $60 \times 60$ matrix.

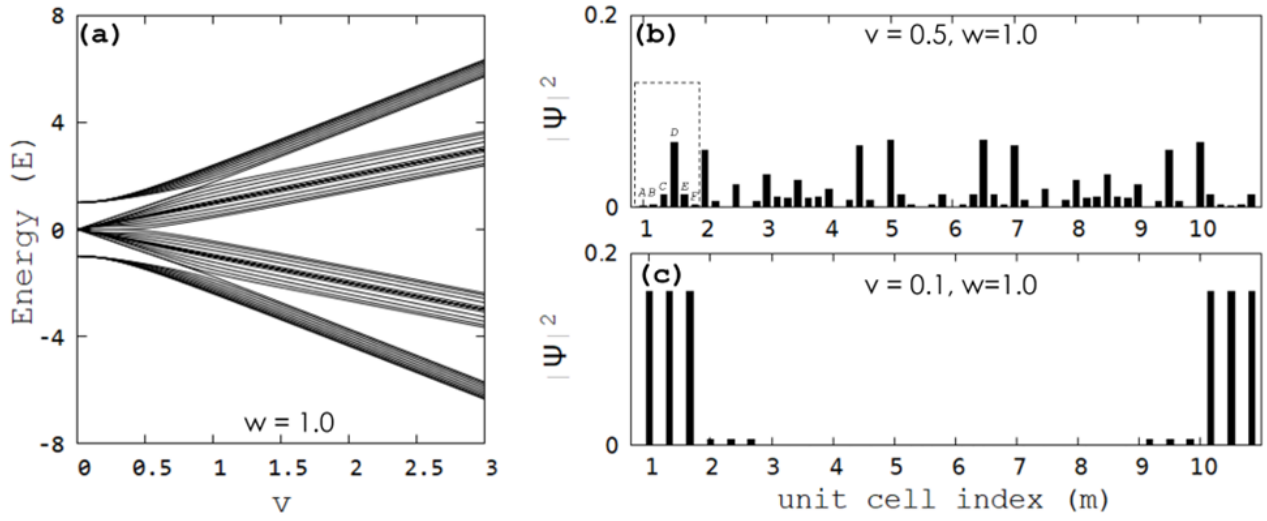


**Figure 11.** Eigenvalues and eigenstates of a finite hexagonal chain with N = 10: [a] energy of N = 10 unit cells hexagonal chain with w = 1 and varying v; [b] probability density of an arbitrary nonzero energy state; [c] probability density of a zero-energy edge state.

Shown in Figure 11a are the eigenvalue spectra obtained by plotting the energy eigenvalues with $w = 1$ and slowly tuning $v$ in the range [0,3]. Furthermore, Figures 11b and c show a representative extended state and an edge state of the finite hexagonal chain. A pair of zero energy edge states (one shown in Figure 11c) show up when $v$ is varied. Additionally, we observe a topological phase transition around $v = 0$. The representative states as seen in Figure 11b shows an arbitrary nonzero energy state. In this figure, it can be seen that the probability density is extended across the chain indicating the conducting characteristics of a trivial topology. In contrast, the edge state shown in Figure 11c indicates that the probability density is localized at the edges of the chain revealing the nontrivial topology of the system.

To establish the bulk-boundary correspondence of the hexagonal chain, we express the bulk momentum-space Hamiltonian in terms of its basis states:

$$H(k) = (w\,cos(k))\zeta_1 + (w\,sin(k))\zeta_2 + (\sqrt{6}v)\zeta_3, \tag{26}$$

where $\zeta_1$, $\zeta_2$, and $\zeta_3$ are:

$$\zeta_1 = \begin{pmatrix} 0 & 0 & 0 & 1 & 0 & 0 \\ 0 & 0 & 0 & 0 & 0 & 0 \\ 0 & 0 & 0 & 0 & 0 & 0 \\ 1 & 0 & 0 & 0 & 0 & 0 \\ 0 & 0 & 0 & 0 & 0 & 0 \\ 0 & 0 & 0 & 0 & 0 & 0 \end{pmatrix}, \zeta_2 = \begin{pmatrix} 0 & 0 & 0 & -i & 0 & 0 \\ 0 & 0 & 0 & 0 & 0 & 0 \\ 0 & 0 & 0 & 0 & 0 & 0 \\ i & 0 & 0 & 0 & 0 & 0 \\ 0 & 0 & 0 & 0 & 0 & 0 \\ 0 & 0 & 0 & 0 & 0 & 0 \end{pmatrix}, \zeta_3 = \frac{1}{\sqrt{6}} \begin{pmatrix} 0 & 1 & 0 & 0 & 0 & 1 \\ 1 & 0 & 1 & 0 & 0 & 0 \\ 0 & 1 & 0 & 1 & 0 & 0 \\ 0 & 0 & 1 & 0 & 1 & 0 \\ 0 & 0 & 0 & 1 & 0 & 1 \\ 1 & 0 & 0 & 0 & 1 & 0 \end{pmatrix}. \tag{27}$$

These matrices satisfy the orthonormality condition $\mathrm{Tr}[\zeta_i \zeta_j] = 2\,\delta_{ij}$. They are three of the 35 matrices representing the basis of the group SU(6). Furthermore, we define the chiral symmetric operator:

$$\Gamma = \begin{pmatrix} 1 & 0 & 0 & 0 & 0 & 0 \\ 0 & -1 & 0 & 0 & 0 & 0 \\ 0 & 0 & 1 & 0 & 0 & 0 \\ 0 & 0 & 0 & -1 & 0 & 0 \\ 0 & 0 & 0 & 0 & 1 & 0 \\ 0 & 0 & 0 & 0 & 0 & -1 \end{pmatrix} \tag{28}$$

where $\Gamma H(k) \Gamma^{\dagger} = -H(k)$ and $\Gamma^2 = 1$. This $6 \times 6$ chiral operator ensures that the energies of the system form chiral symmetric pairs.

The trajectories of the bulk momentum-space Hamiltonian of the hexagonal chain in ζ-space, Equation 26 with varying hopping parameters are shown in Figure 9b. The trajectory of Equation 26 forms a cylindrical plot with radius $w$ and height $v$. Thus, increasing the value of $w$ and $v$ will increase the radius and height, respectively. The same as the procedure introduced in the previous section, we determine the winding number to be:

$$\nu = \begin{cases} 1, & v = 0 \\ 0, & v = 0.5 \\ 0, & v = 1 \end{cases}, \tag{29}$$

where we keep the value of $w = 1$. As seen from the calculation of the winding number, we expect a pair of localized edge states in the region $v = 0$, where the winding number $\nu = 1$. An example of this edge state is shown in Figure 11c.

## CONCLUSION

In summary, we extended the SSH model into three distinct types – the trimer chain, the generalized trimer chain, and the hexagonal chain. The trimer chain is a one-dimensional lattice with sites $A$,$B$, and $C$ and staggered hopping potentials $v$ and $w$ for the intracell and intercell hopping energies. The generalized trimer chain is a generalization of the trimer chain with the hopping parameters $v_1, v_2, w_1$, and $w_2$ to distinguish the $A$ to $B$ and $A$ to $C$ hopping. Lastly, the hexagonal chain is composed of six sublattices with staggered hopping potentials $v$ and $w$ for the intracell and intercell hopping.

Exact diagonalization was used to calculate the energy eigenvalues of the bulk and the finite systems of the extended models. For the trimer chain, we find that the bulk characteristic of the chain exhibits conducting characteristics due

to the flat band situated along the fermi energy independent of the values of $v$ and $w$. Furthermore, when the hopping potentials are equal, it is seen that the uppermost and lowermost bands meet at $k = \pm\pi$. The trimer chain's finite structure shows the presence of gapless zero-energy edge states as well as a topological phase transition, properties that resemble the characteristics of a one-dimensional TI. The bulk-boundary correspondence for the trimer chain also predicts the existence of these localized edge states through the winding number $\nu$ where we determine $\nu = 1$ in the topological ($v < w$) regime. The bulk characteristic of the generalized trimer chain, on the other hand, also shows conducting characteristics due to the flat band situated along the Fermi level. In the generalized case, where $v_1 \neq w_1$ and/or $v_2 \neq w_2$, a visible band gap can be seen between the uppermost and the lowest bands. This band gap only closes at the limit when $v_1 = w_1$ and $v_2 = w_2$. The bulk-boundary correspondence of the generalized trimer chain reveals that the gapless topological edge states (localized on both edges) are only present in the trimer chain limit when $v_1 = v_2$. Gapped chiral edge states on the other hand, *i.e.* localized only on the left or right boundary, show up in the region where $(v_1 \neq v_2) < (w_1 = w_2)$. Lastly, for the hexagonal chain, the dispersion relations show that the model is semi-metal when $v < w$ due to the absence of band gap and a metal when $v = 0$ due to the presence of degenerate flat bands at the Fermi level. The existence of gapless localized edge states is also observed in the finite hexagonal chain at around $v = 0$, where the system is in the topological phase defined by a winding number $\nu = 1$.

## ACKNOWLEDGMENT

The authors are grateful to Rafael Bautista for insightful discussions.

## REFERENCES

ASBOTH J, OROSZLANY L, PALYI A. 2015. A short course on topological insulators: band structure topology in one and two dimension. arXiv 1509: 02295v1.

BERCIOUX D, DUTTA O, RICO E. 2017. Solitons in one-dimensional lattices with flat band. Annalen der Physik 529(9): 1600262.

FUJITA M, IGAMI M, NAKADA K. 1997. Lattice distortion in nanographite ribbons. Journal of the Physical Society of Japan 6: 1864–1867.

GNU PROJECT. 2024. GNU Octave, version 8.4.0. GNU. Accessible at https://www.gnu.org/software/octave/

GUO H. 2016. A brief review of one-dimension topological insulators and superconductors. Science China Physics, Mechanics, & Astronomy 59: 637401.

HABER H. 2017. Properties of the Gell-Mann matrices. In: Physics 251 Group Theory and Modern Physics. UC Santa Cruz. Retrieved on 11 Aug 2024 from http://scipp.ucsc.edu/~haber/archives/physics251_17/gellmann17.pdf

HASAN MZ, KANE K. 2010. Colloquim: topological insulators. Reviews in Modern Physics 82(4): 3045–3067.

MARTINEZ ALVAREZ VM, COUTINHO-FILHO MD. 2019. Edge states in trimer lattices. Phys Rev A 99: 013833.

MOORE JE. 2010. The birth of topological insulators. Nature 464: 194–198.

OBANA D, LIU F, WAKABAYASHI K. 2019. Topological edge states in the Su-Schrieffer-Heeger model. Physical Review B 100: 075437.

SIMON S. 2013. The Oxford solid state basics, 1st ed. Oxford, UK: Oxford University Press. p. 173–181.

SU W, SCHRIEFFER J, HEEGER A. 1979. Solitons in Polyacetylene. Physical Review Letters 42: 1698.

WAN X, TURNER A, VISHWANATH A, SAVRASOV S. 2011. Topological semimetal and Fermi-arc surface states in the electronic structure of pyrochlore iridates. Phys Rev B 83: 205101.

WEN X. 2004. Quantum field theory of many-body systems. Oxford, UK: Oxford University Press. p. 335–352.